Scattering-Based Geometric Shaping of Photon-Photon Interactions

Shahaf Asban* and Shaul Mukamel†
Department of Chemistry and Physics and Astronomy, University of California, Irvine, California 92697-2025, USA

(Received 19 June 2019; revised manuscript received 27 November 2019; published 26 December 2019)

We construct an effective Hamiltonian of interacting bosons, based on scattered radiation off vibrational modes of designed molecular architectures. Making use of the infinite yet countable set of spatial modes representing the scattering of light, we obtain a variable photon-photon interaction in this basis. The effective Hamiltonian Hermiticity is controlled by a geometric factor set by the overlaps of spatial modes. Using this mapping, we relate intensity measurements of the light to correlation functions of the interacting bosons evolving according to the effective Hamiltonian, rendering local as well as nonlocal observables accessible. This architecture may be used to simulate the dynamics of interacting bosons, as well as a designing tool for multiqubit photonic gates in quantum computing applications. Variable hopping, interaction, and confinement of the active space of the bosons are demonstrated on a model system.

DOI: 10.1103/PhysRevLett.123.260502

Quantum machines are fundamentally different from their classical counterparts [1]. Classical computers are implemented using a binary basis set. One of the benefits of this choice is minimal average energy consumption [2], as well as minimal bit error rate in the information transmission of a noisy channel [3]. For such a machine to be useful, it requires large scale integration of fundamental operations, where each level adds to the overall error rate. Deterministic intermediate quantities can be measured and corrected via feedback loops without interrupting the calculation process. In quantum machines, the smallest possible unit of data (qubit) carries a phase that manifests a continuous degree of freedom. Upscaling of operations on qubits is also required for nontrivial tasks. The propagation of quantum information through such integrated system evolves errors continuously as well. This makes the realization of fault tolerant quantum processing challenging and continues to motivate intense scientific effort [4–6]. Quantum simulators based on optical traps pioneered by Cirac, Zoller, and co-workers [7,8] have matured experimentally [9,10]. They are widely used in the study of quantum dynamics, such as spin frustration [10] and thermalization and localization transitions [11,12]. Recently, more applications of lattice gauge theories have been proposed, appealing to simulations of high energy physics [13–15]. While these fascinating quantum simulators offer an unprecedented glimpse into nonequilibrium dynamics, upscaling the number of qubits is just as challenging.

Here we propose a geometric scattering-based spatial photon coupler (SPC) that can be used to simulate quantum dynamics of interacting bosons. The setup is depicted in Fig. 1 and based on "off-resonant scattering" of photons on geometrically arranged distribution of molecules. We show that the scattering process can be mapped into the effective Hamiltonian,

$$H_{\mathrm{eff}} = \sum_{nk} \Theta_{nk} a_n^\dagger a_k - \sum_{nklm} U_{nklm} a_n^\dagger a_k a_l^\dagger a_m, \qquad (1)$$

where $a_k(a_k^\dagger)$ is a discrete bosonic annihilation (creation) operator. The hopping (Θ_{nk}) and the interaction (U_{nklm}) terms are determined by three main quantities: (1) the geometry (design) of the microscopic building blocks, (2) their internal structure (spectrum), and (3) the measurement basis chosen. It holds two significant advantages. First, it can be designed to maintain Hermiticity such that marginal losses in photon number occur [16]; inelastic contributions in this case result in a frequency shift of the incident photon. Second, while the number of connected modes is infinite, it can be confined with intelligent design. Our goal is to shape the induced dynamics constrained by the Hamiltonian in Eq. (1), then read the encoded information from the final photonic wave function,

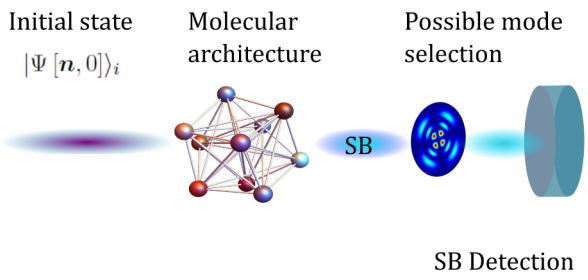

FIG. 1. Proposed realization of the geometric SPC. The incident beam is scattered off a molecular architecture, realizing interaction between its spatial components, denoted SB. A single mode as well as any combination of such are addressable, rendering projective measurement in the chosen basis possible. The SBs can be mapped into discrete lattice sites for which cross-correlations can be constructed using the photon statistics.

$$|\Psi[\boldsymbol{n},\tau]\rangle_f = e^{-iH_{\rm eff}\tau}|\Psi[\boldsymbol{n},0]\rangle_i. \tag{2}$$

Intensity measurements reveal the scattered bosons (SBs) densities $\hat{n}_k \equiv a_k^\dagger a_k$, evolving on a network (graph) of a topology imposed by $H_{\rm eff}$ connectivity as depicted in Fig. 1. τ denotes the interaction time, beyond which $U_{nklm} \equiv 0$.

We consider arbitrary initial superposition of spatial modes, reflecting some initial (multiple-photon) distribution of SBs. One possibility of particular interest to the simulation of interacting bosons is a (normalized) product of N single-photon states $|\mathbf{1}\rangle = \sum_n C_n a_n^\dagger|0\rangle$, corresponding to initially noninteracting bosons. One way to achieve that is by direct state preparation. Another is via two-mode spontaneous parametric down-converter source in which one photon is scattered while the other serves as the reference for the SB (RSB) as was done in [17] and inspired by [18–22] (see [23]). In both manifestations, the RSBs are used to extract the SB statistics, which is first scattered as depicted in Fig. 1. Surveying the SBs statistics using cross-correlations with RSBs, renders "local" $\propto \langle\hat{n}_r(\tau)\rangle$ and $\langle\hat{n}_r(0)\hat{n}_r(\tau)\rangle$, as well as "nonlocal" quantities $\propto \sum_R \langle\hat{n}_r(0)\hat{n}_{r+R}(\tau)\rangle$ accessible. While conventional quantum simulators are limited by the number of physical qubits, the proposed geometric SPC benefits from controlled—potentially infinite—number of participating modes. These characteristics are highly desirable for simulating thermodynamic properties of interacting particles.

Constructing the effective Hamiltonian.—Off-resonant light-matter interaction is given by the minimal coupling Hamiltonian,

$$H_{\mu\phi} = \int d\boldsymbol{r}\sigma(\boldsymbol{r},t)\boldsymbol{A}^2(\boldsymbol{r},t), \tag{3}$$

where μ and ϕ denote the matter and photon fields, respectively. The interaction of radiation modes is mediated by the charge-density operator $\sigma(\boldsymbol{r})$. The vector potential in the paraxial approximation takes the form $\boldsymbol{A}_p(\boldsymbol{r},t) = \sum_{\sigma,l,p}\int_0^\infty dk_0 C(k_0)[A^{(+)}_{\sigma lp}(k_0)e^{ik_0(z-ct)} + \text{H.c.}]$, where k_0 is the wave vector in the longitudinal direction, $C(k_0) = (1+\vartheta^2/16\pi^3\varepsilon_0 k_0)^{1/2}$ and $\vartheta = q/\sqrt{2k_0^2}$ is the degree of paraxiality [24,25]. The vector potential operator is defined by $A^{(+)}_{\sigma lp}(k_0) = \epsilon_\sigma \hat{a}_{\sigma,l,p}(k_0)\psi_{l,p}(\boldsymbol{\rho},z;k_0)$, where $\hbar = c = 1$. $\boldsymbol{\rho}$ is the polar distance (cylindrical coordinates) and the indices l, p label the spatial basis set $\psi_{lp}(\boldsymbol{\rho},z;k_0)$ [in [24,25], the Laguerre-Gauss (LG) basis is used]. Any complete basis that is a solution of the paraxial equation, such as Hermite-Gauss (HG) or Ince-Gauss can be used. Here $\epsilon_\sigma = (\boldsymbol{u}_x - i\sigma\boldsymbol{u}_y)/\sqrt{2}$ is the polarization vector [circular for LG modes (linear for HG)] and $\sigma = \pm 1$. The field (creation and annihilation) operators in the paraxial basis satisfy the canonical commutation relations $[\hat{a}_{\sigma,l,p}(k_0), \hat{a}^\dagger_{\sigma',l',p'}(k_0')] = \delta_{\sigma\sigma'}\delta_{ll'}\delta_{pp'}\delta(k_0-k_0')$. The paraxial basis is given by the transformation of the standard operators $\hat{a}_{\sigma,l,p}(k_0) = \int d^2\boldsymbol{q}\phi^*_{lp}(\boldsymbol{q})\hat{a}_\sigma(\boldsymbol{q})$. This basis has the following properties:

$$\sum_{l,p}\phi^*_{lp}(\boldsymbol{q})\psi_{lp}(\boldsymbol{\rho},z,k_0) = e^{i\boldsymbol{q}\cdot\boldsymbol{\rho}-k_0\vartheta^2 z}, \tag{4a}$$

$$\int d^2\boldsymbol{q}\phi^*_{lp}(\boldsymbol{q})\phi_{mn}(\boldsymbol{q}) = \delta_{lm}\delta_{pn}, \tag{4b}$$

$$\sum_{l,p}\phi^*_{lp}(\boldsymbol{q})\phi_{lp}(\boldsymbol{q}') = \delta(\boldsymbol{q}-\boldsymbol{q}'), \tag{4c}$$

where $\boldsymbol{q}$ is the transverse momentum and $\phi_{lp}(\boldsymbol{q})$ is the LG spatial modes Fourier transform taken at $z = 0$. The full Hamiltonian is given by $\mathcal{H} = H_0 + H_{\mu\phi}$, where $H_0 = H_\phi + H_\mu$ is the noninteracting Hamiltonian of the radiation (ϕ) and matter (μ). With these notations, the interaction Hamiltonian can be recast in the form

$$H_{\mu\phi} = \sum_{\boldsymbol{kq}}\sigma^\dagger_{\boldsymbol{k}-\boldsymbol{q}}a^\dagger_{\boldsymbol{k}}a_{\boldsymbol{q}} + \sigma_{\boldsymbol{k}-\boldsymbol{q}}a_{\boldsymbol{k}}a^\dagger_{\boldsymbol{q}}, \tag{5}$$

where the highly oscillating terms corresponding to $a_{\boldsymbol{k}}a_{\boldsymbol{q}}$ and $a^\dagger_{\boldsymbol{k}}a^\dagger_{\boldsymbol{q}}$ are neglected. The matter Hamiltonian is given by $H_\mu = \sum_{\alpha,i}\epsilon_{i,\alpha}c^\dagger_{i,\alpha}c_{i,\alpha}$, where $c_{i,\alpha}(c^\dagger_{i,\alpha})$ is the bosonic annihilation (creation) operator with the canonical commutation relations $[c_{i,\alpha}, c^\dagger_{j,\beta}] = \delta_{\alpha\beta}\delta_{i,j}$. The vibrational modes are labeled i and scatters by α. The charge-density operator reads $\sigma_{\boldsymbol{k}} = \sum_{\alpha=1}^N f_\alpha(\boldsymbol{k})c^\dagger_{i,\alpha}c_{j,\alpha}$, where $f_\alpha(\boldsymbol{k}) = e^{i\boldsymbol{k}\cdot\boldsymbol{r}_\alpha}w(\boldsymbol{k})$, $w(\boldsymbol{k})$ are the localized molecular orbital and $\boldsymbol{r}_\alpha$ are scatterer's positions. We then calculate the effective photon-photon interaction using the Schrieffer-Wolff transformation [see Appendix (B.1) of the Supplemental Material [26] for detailed derivation], follows by a transformation of the momentum representation into superposition the SBs.

The SB representation.—Using the above definitions for the Bogoliubov transformation from momentum space to the Schmidt representation $a_{\boldsymbol{k}} = \sum_n \phi_n(\boldsymbol{k})a_n$, where a_n is the Schmidt boson annihilation operator and n is a shorthand notation for the two quantum numbers l, p introduced in the expression for the vector potential. The free Hamiltonian reads, assuming a single longitudinal mode at ω_0, $H_\phi = \omega_0\sum_n a^\dagger_n a_n$. The off-diagonal contributions to Eq. (1)—namely, the hopping terms—are given by (see Supplemental Material [26] for detailed derivation),

$$\hat{t}_{\rm coh} = \sum_{nm}\theta^{\rm coh}_{nm}a^\dagger_n a_m + \text{H.c.}, \tag{6a}$$

$$\hat{t}_{\rm inc} = \sum_{nm}\theta^{\rm inc}_{nm}(\Delta_i)a^\dagger_n a_m + \theta^{\rm inc*}_{nm}(-\Delta_i)a^\dagger_m a_n, \tag{6b}$$

with the hopping coefficients

$$\theta_{nm}^{\mathrm{coh}} = 2\sum_{\alpha\neq\beta}\sum_{\boldsymbol{k},\boldsymbol{q},\boldsymbol{s}} e^{-i(k-\boldsymbol{q})\cdot\boldsymbol{r}_\alpha + i(\boldsymbol{s}-\boldsymbol{q})\cdot\boldsymbol{r}_\beta} \times \frac{\phi_n^*(\boldsymbol{k}) w_\alpha^*(\boldsymbol{k}-\boldsymbol{q}) w_\beta(\boldsymbol{s}-\boldsymbol{q})\phi_m(\boldsymbol{s})}{q^2-k^2}, \tag{7a}$$

$$\theta_{nm}^{\mathrm{inc}}(\Delta_i) = 2\sum_{\alpha}\sum_{\boldsymbol{k},\boldsymbol{q},\boldsymbol{s}} e^{-i(\boldsymbol{k}-\boldsymbol{s})\cdot\boldsymbol{r}_\alpha} \times \frac{\phi_n^*(\boldsymbol{k}) w_\alpha^*(\boldsymbol{k}-q') w_\alpha(\boldsymbol{q}-\boldsymbol{q}')\phi_m(\boldsymbol{s})}{q'^2-(k^2+\Delta_i)}, \tag{7b}$$

and $\Delta_i = 2\omega_0\epsilon_{ig}$. Assuming a slowly varying orbital in momentum domain (point particle limit) significantly simplifies Eqs. (7a) and (7b). When the interparticle distance is much smaller than the transverse wave vector $r_{\alpha\beta} \ll \lambda_\perp$, the coherent hopping [Eq. (7a)] is granted an intuitive form, carrying spatial contributions due to the phase difference of scattered modes. Introducing a cutoff frequency Λ such that $|r_{\beta\alpha}|/\Lambda \leq |r_{\beta\alpha}|k \ll 1$ and $q > 1/\Lambda$, we obtain

$$\theta_{nm}^{\mathrm{coh}} = g^{\mathrm{coh}}\sum_{\alpha\neq\beta}\psi_n^*(\boldsymbol{r}_\alpha)\psi_m(\boldsymbol{r}_\beta), \tag{8a}$$

$$\theta_{nk}^{\mathrm{inc}} = g^{\mathrm{inc}}\sum_{\alpha}\psi_n^*(\boldsymbol{r}_\alpha)\psi_k(\boldsymbol{r}_\alpha). \tag{8b}$$

Note that these approximations are not essential, yet they grant important intuition; see Appendix B for the exact expressions. The overall SB hopping coefficient is given by $\Theta_{nk} = \omega_0(\delta_{nk} - \theta_{nk}^{\mathrm{coh}} - \theta_{nk}^{\mathrm{inc}})$.

The interaction term in Eq. (1) can be displayed in a form that separates the geometrical factor from the basis-dependent one $U_{nmls} = -\sum_{l's'} S_{ll'ss'} V_{nml's'}$. Here V_{nlkm} is the basis-dependent four-mode "scattering potential"

$$V_{nlkm} = \sum_i \int d^2\boldsymbol{k} d^2\boldsymbol{q}\, \phi_n^*(\boldsymbol{k})\phi_k(\boldsymbol{k}) \times \left(\frac{1}{k^2-q^2-\Delta_i} - \frac{1}{k^2-q^2+\Delta_i}\right)\phi_l(\boldsymbol{q})\phi_m^*(\boldsymbol{q}), \tag{9}$$

and the geometric structural tensor $S_{ll'ss'} = \sum_\alpha f_{ll'}^{\alpha *} f_{ss'}^{\alpha}$, using concatenation of basis $\leftrightarrow$ geometry transformation $f_{nm}^{\alpha} = \psi_n^*(r_\alpha)\psi_m(r_\alpha)$, isolating basis-dependent properties from the geometric characteristics. The effective Hamiltonian is finally given by Eq. (1).

The scattering potential in the Laguerre-Gauss basis.—The target effective interaction to be simulated is manipulated and designed using three main ingredients: (i) purely geometric and defined by the arrangement of charges, (ii) the internal structure of each charge (Δ_i), and (iii) the choice of basis. While the geometric component appears in the expressions for both the interaction and hopping terms, the charge spectral structure contributes to the scattering potential of Eq. (9) alone. We now study the effects of Δ on the interaction that is basis dependent yet geometry independent. The scattering potential V_{nklm} involves coupling between four modes. Equation (9) can be further simplified using the LG basis [see Eq. (35B) of the Supplemental Material [26]]. The structure of the scattering potential as a function of Δ for a two-level system is depicted in Fig. 2. For all values of Δ, the relation between the first and last two modes [n, k and l, m of Eq. (1)] resembles a Kronecker delta. It is given by the partial traces $V_{nm} = \mathrm{tr}_{kl} V_{nmkl} \approx \delta_{nm}$ and $V_{kl} = \mathrm{tr}_{nm} V_{nmkl} \approx \delta_{kl}$ and depicted in Fig. 2(a). This property simplifies the effective Hamiltonian to

$$H_{\mathrm{eff}}^{\mathrm{LG}} = \sum_{n,k}\Theta_{nk} a_n^\dagger a_k - \sum_{nk}\mathcal{U}_{nk}\hat{n}_n\hat{n}_k, \tag{10}$$

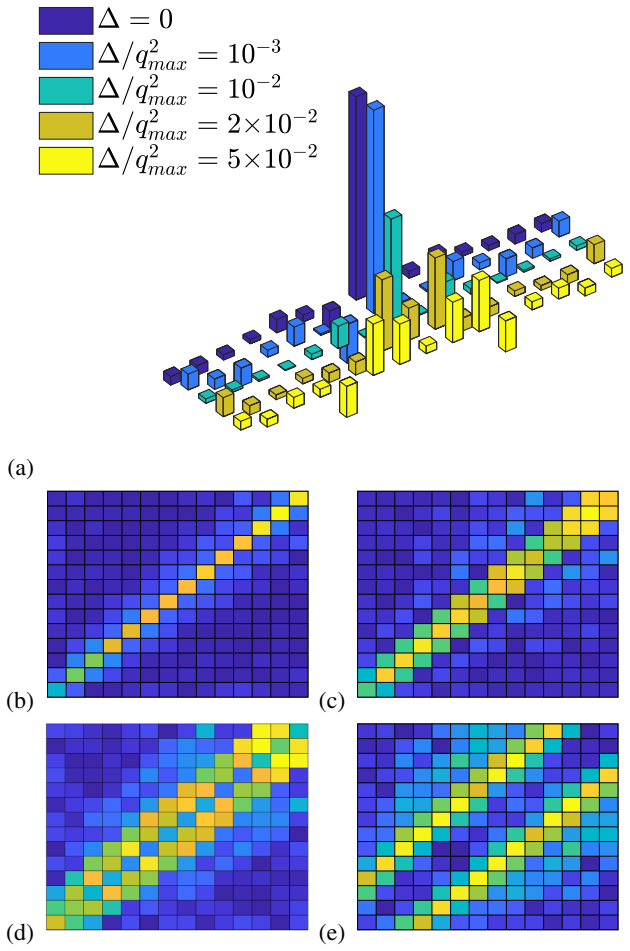

FIG. 2. The scattering potential. V_{nmkl} in Eq. (9) calculated in the LG basis. (b)–(e) Correspond to different Δ value, and (a) captures a summary of the diagonal cross section from the top left to bottom right of panels (b)–(e). Panels (b)–(e) capture the intermode coupling [relations between the two middle dimensions $(V_{mk} = \mathrm{tr}_{nl} V_{nmkl})$] of the effective SBs scattering potential for the selected values $\Delta/\boldsymbol{q}_{\mathrm{max}}^2 = (0.001, 0.01, 0.02, 0.05)$. The calculated relations between the first two $(V_{nm} = \mathrm{tr}_{kl} V_{nmkl})$ and last dimensions $(V_{kl} = \mathrm{tr}_{nm} V_{nmkl})$ are indistinguishable from (b) for all values of Δ and resemble a Kronecker delta distribution.

where $\hat{n}_k = a_k^\dagger a_k$ is the number operator and $\mathcal{U}_{nk} = \sum_{lm} U_{nlkm}\delta_{nl}\delta_{km}$. The effective potential between the first and last two modes of Eq. (1) spreads to neighboring modes with increasing values of $\Delta/\boldsymbol{q}_{\max}^2$, where $\boldsymbol{q}_{\max}$ is the cutoff wave vector in the numerical calculation. This behavior is summarized in Fig. 2(a) and demonstrated separately for the selected values in Figs. 2(b) and 2(e). At large values of $\Delta/\boldsymbol{q}_{\max}^2$ the scattering occurs between more distant modes, corresponding to energy exchange with the matter. Extension of this result to a system of charges composed of a more complex internal structure is given by a straightforward summation, resulting in longer-range interaction.

Illustrative example of the effective Hamiltonian.—We derive the effective Hamiltonian for molecules in cylindrical architecture, in which controlled hopping can confine the dynamics to a restricted subspace. We consider a uniform distribution of molecules filling a hollow cylinder (UC) of inner radius a and outer radius b as shown in Fig. 3. The boundary radius c is defined such that 95% of the power of the incident radial mode for which $n = 25$ is contained within the calculation range of the numerical simulation (the chosen cutoff mode).

In this case, the geometric coefficient of the hopping terms in Eqs. (8a) and (8b) as well as the interaction can be used to confine the dynamics in a controlled subspace. By varying a and b, the hopping range depicted in Figs. 4(a) and 4(d) can be controlled. Figure 4 along with Eqs. (8a) and (8b) show that hopping within the set of modes corresponding to the positive geometric factor is energetically favorable. These positive contributions are surrounded by negative ones, which are costly energetically, resulting in effective confinement. In this setup, the single-molecule field scattering presented in Eq. (8b) dominates the hopping dynamics and the coherent hopping term of Eq. (8a) is suppressed. This is verified by the vanishing structure factor in a disordered lattice or, equivalently, from the closure relations of the LG basis combined with orthogonality [Eqs. (4c) and (4b)]. Using Eq. (4a) one can estimate that for $|\boldsymbol{q}_{\max}| = 10^{-p}k_0$ and $\Delta z = 10^l\lambda_0$ the modal attenuation factor is $\exp(-2\pi 10^{l-2p})$, which yields $\approx 94\%$ of the incoming photon flux at the output for $l = p = 2$. This geometry simulates the dynamics of the Hamiltonian $H_{\text{eff}}^{\text{LG}} = H_{\text{UC}}$,

$$H_{\text{UC}} = \sum_{\langle n,k\rangle \in \mathcal{D}_h} \Theta_{nk} a_n^\dagger a_k - \sum_{n,k\in\mathcal{D}_\Delta} \mathcal{U}_{nk}\hat{n}_n\hat{n}_k, \tag{11}$$

where $\langle n, k\rangle$ stands for nearest neighbors. $\mathcal{D}_h$ is a domain determined by the geometry in which the hopping occurs, as shown in Fig. 4. $\mathcal{D}_\Delta$ is the domain set by Δ for which several illustrations are depicted in Fig. 2.

Discussion.—We have developed a geometric SPC, shaping photon-photon interactions via geometric design of the coupling between spatial modes, using the setup depicted in Fig. 1. Quantum dynamics of interacting bosons described by the Hamiltonian of Eq. (1) can be simulated and directly measured using the above ingredients.

The dynamics of the SBs constrained by the Eq. (1) is controlled by the following three main quantities: the geometric distribution of molecules, their internal structure, and the choice of spatial basis. The dynamics induced by the geometric SPC depicted in Fig. 3 can be restricted to a finite set of modes as demonstrated in Fig. 4. This offers a "purpose-computing platform" to a class of problems with exponential complexity. There is a growing interest in purpose machines, built for the solution of a specific task, e.g., coherent Ising machines [27,28]. These structures are designed to solve efficiently Ising models on graphs with programmable connectivity. Their usefulness stems from the well-known mapping between the Ising model ground state search problem and combinatorial optimization problems in polynomial time [29] (both nondeterministic

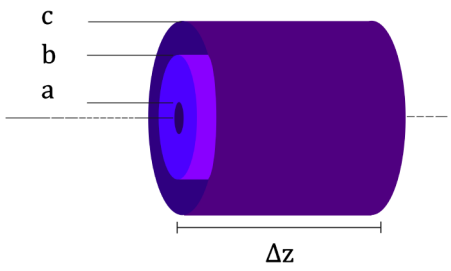

FIG. 3. Uniformly distributed hollow cylinder. Inner and outer radius a and b, respectively; c is chosen such that 95% of the power of the radial mode for which $n = 25$ is contained within. Δz is the region in which the interaction and hopping occur, corresponding to the interaction time interval τ.

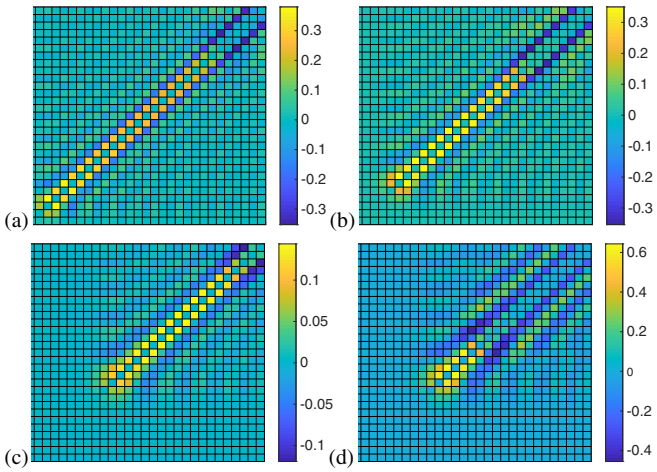

FIG. 4. Geometrically controlled hopping confinement. (a)–(d) The geometric hopping factors θ_{nk}^{inc} presented in Eq. (8b) are displayed for the above geometry. (a)–(d) Computed with the corresponding dimensionless distance from the origin $(a/c, b/c)$: [(a) (0.1,0.9), (b) (0.2,0.8), (c) (0.4,1), (d) (0.4, 0.6)]. Positive contributions are energetically favorable.

polynomial-time hardness). The proposed setup is also applicable as a quantum (light) state-preparation technique, as well as a multiphoton gate in a photonic quantum processor.

In molecular systems, the number of vibrational modes N_{vib} is proportional to the number of atoms N_a according to $N_{\mathrm{vib}} = 3N_a - 6$. The number of electronic states corresponds to the number of electrons N_e. Good candidates would be systems containing few vibrational modes while having a large number of electrons that potentially provide strong coupling of the vibrational modes with an applied electromagnetic field. Short wavelength tabletop x-ray sources that couple off-resonantly between the vibrational modes provide intriguing possibility for source realization [30]. Longer wavelength sources for which sophisticated measurement techniques are more mature may be possible, although the coupling between the modes may take more complicated forms.

Because of the structure of the LG modes, for a low number of ordered scatterers, sign-flipping antiferromagnetic coupling has been observed that requires further characterization. Finding the molecular distribution and basis emulating the desired dynamics provides a topic for future study, as well as coupling to electronic states rather than the vibrational. For this purpose, another degree of the geometric properties could be considered, the local charge distribution of each scatterer presented in Eqs. (7a) and (7b).

The support of the Chemical Sciences, Geosciences, and Biosciences Division, Office of Basic Energy Sciences, Office of Science, U.S. Department of Energy is gratefully acknowledged. S. M. was supported by Award No. DE-FG02-04ER15571. S. A. was supported by a National Science Foundation Fellowship (Grant No. CHE-1663822).

*Shahaf.S.Asban@gmail.com
†smukamel@uci.edu

[1] M. A. Nielsen and I. L. Chuang, *Quantum Computation and Quantum Information: 10th Anniversary Edition* (Cambridge University Press, Cambridge, England, 2010).
[2] Assuming voltage levels are assigned to bit states, having "0" represented by zero voltage.
[3] P. Massoud Salehi and J. Proakis, *Digital Communications* (McGraw-Hill Education, New York, 2007).
[4] P. W. Shor, Scheme for reducing decoherence in quantum computer memory, Phys. Rev. A **52**, R2493 (1995).
[5] D. Gottesman, A. Kitaev, and J. Preskill, Encoding a qubit in an oscillator, Phys. Rev. A **64**, 012310 (2001).
[6] P. Schindler, J. T. Barreiro, T. Monz, V. Nebendahl, D. Nigg, M. Chwalla, M. Hennrich, and R. Blatt, Experimental repetitive quantum error correction, Science **332**, 1059 (2011).
[7] J. I. Cirac and P. Zoller, Quantum Computations with Cold Trapped Ions, Phys. Rev. Lett. **74**, 4091 (1995).
[8] D. Jaksch, C. Bruder, J. I. Cirac, C. W. Gardiner, and P. Zoller, Cold Bosonic Atoms in Optical Lattices, Phys. Rev. Lett. **81**, 3108 (1998).
[9] C. Monroe, Quantum information processing with atoms and photons, Nature (London) **416**, 238 (2002).
[10] K. Kim, M.-S. Chang, S. Korenblit, R. Islam, E. E. Edwards, J. K. Freericks, G.-D. Lin, L.-M. Duan, and C. Monroe, Quantum simulation of frustrated Ising spins with trapped ions, Nature (London) **465**, 590 (2010).
[11] M. Schreiber, S. S. Hodgman, P. Bordia, H. P. Lüschen, M. H. Fischer, R. Vosk, E. Altman, U. Schneider, and I. Bloch, Observation of many-body localization of interacting fermions in a quasirandom optical lattice, Science **349**, 842 (2015).
[12] J. Smith, A. Lee, P. Richerme, B. Neyenhuis, P. W. Hess, P. Hauke, M. Heyl, D. A. Huse, and C. Monroe, Many-body localization in a quantum simulator with programmable random disorder, Nat. Phys. **12**, 907 (2016).
[13] E. Zohar, J. I. Cirac, and B. Reznik, Quantum simulations of lattice gauge theories using ultracold atoms in optical lattices, Rep. Prog. Phys. **79**, 014401 (2016).
[14] E. Rico, M. Dalmonte, P. Zoller, D. Banerjee, M. Bogli, P. Stebler, and U.-J. Wiese, So(3) "nuclear physics" with ultracold gases, Ann. Phys. (Amsterdam) **393**, 466 (2018).
[15] C. Muschik, M. Heyl, E. Martinez, T. Monz, P. Schindler, B. Vogell, M. Dalmonte, P. Hauke, R. Blatt, and P. Zoller, U(1) Wilson lattice gauge theories in digital quantum simulators, New J. Phys. **19**, 103020 (2017).
[16] In linear order of the paraxiality parameter ϑ there are *no losses* in the longitudinal modes. Losses in the transverse modes are governed solely by the geometry. Higher orders exhibit losses, see discussion in the illustrative example of the effective Hamiltonian.
[17] S. Asban, K. E. Dorfman, and S. Mukamel, Quantum phase-sensitive diffraction and imaging using entangled photons, Proc. Natl. Acad. Sci. U.S.A. **116**, 11673 (2019).
[18] R. Fickler, G. Campbell, B. Buchler, P. K. Lam, and A. Zeilinger, Quantum entanglement of angular momentum states with quantum numbers up to 10 010, Proc. Natl. Acad. Sci. U.S.A. **113**, 13642 (2016).
[19] R. Fickler, R. Lapkiewicz, W. N. Plick, M. Krenn, C. Schaeff, S. Ramelow, and A. Zeilinger, Quantum entanglement of high angular momenta, Science **338**, 640 (2012).
[20] M. Krenn, R. Fickler, M. Huber, R. Lapkiewicz, W. Plick, S. Ramelow, and A. Zeilinger, Entangled singularity patterns of photons in Ince-Gauss modes, Phys. Rev. A **87**, 012326 (2013).
[21] J. Bavaresco, N. Herrera Valencia, C. Klöckl, M. Pivoluska, P. Erker, N. Friis, M. Malik, and M. Huber, Measurements in two bases are sufficient for certifying high-dimensional entanglement, Nat. Phys. **14**, 1032 (2018).
[22] S. S. Straupe, D. P. Ivanov, A. A. Kalinkin, I. B. Bobrov, and S. P. Kulik, Angular schmidt modes in spontaneous parametric down-conversion, Phys. Rev. A **83**, 060302(R) (2011).
[23] Using an entangled photon pair such as SB and RSB ideally results in a background-free signal, yet is harder to produce.
[24] A. Aiello and J. P. Woerdman, Exact quantization of a paraxial electromagnetic field, Phys. Rev. A **72**, 060101(R) (2005).

[25] G. F. Calvo, A. Picon, and E. Bagan, Quantum field theory of photons with orbital angular momentum, Phys. Rev. A **73**, 013805 (2006).

[26] See Supplemental Material at http://link.aps.org/supplemental/10.1103/PhysRevLett.123.260502 for the derivation of the effective Hamiltonian including: Hopping terms in Eqs. (6a) and (6b), their coefficients in Eqs. (7a) and (7b) and their approximated form of Eqs. (8a) and (8b) and the general scattering potential in Eq. (9) as well as the LG mode expansion in Eq. (10).

[27] T. Inagaki, Y. Haribara, K. Igarashi, T. Sonobe, S. Tamate, T. Honjo, A. Marandi, P. L. McMahon, T. Umeki, K. Enbutsu, O. Tadanaga, H. Takenouchi, K. Aihara, K.-i. Kawarabayashi, K. Inoue, S. Utsunomiya, and H. Takesue, A coherent Ising machine for 2000-node optimization problems, Science **354**, 603 (2016).

[28] P. L. McMahon, A. Marandi, Y. Haribara, R. Hamerly, C. Langrock, S. Tamate, T. Inagaki, H. Takesue, S. Utsunomiya, K. Aihara, R. L. Byer, M. M. Fejer, H. Mabuchi, and Y. Yamamoto, A fully programmable 100-spin coherent Ising machine with all-to-all connections, Science **354**, 614 (2016).

[29] F. Barahona, On the computational complexity of Ising spin glass models, J. Phys. A **15**, 3241 (1982).

[30] J. J. Rocca, Table-top soft x-ray lasers, in *Conference on Lasers and Electro-Optics* (Optical Society of America, Washington, DC, 2016), p. AM1K.1.

Supplementary materials for "Scattering-based geometric shaping of photon-photon interactions"

Our goal is to construct controlled interaction between these modes that will emulate the one of a desired quantum system. For this, we consider the setup in which initially entangled beam given by a certain Schmidt decomposition interacts with the charge distribution (CD).

Appendix A: Full Hamiltonian of Schmidt bosons

This is a straightforward derivation of the light matter coupling in the Schmidt basis. It is exact and therefore the effective interaction is not clearly pronounced.

The interaction Hamiltonian for a flat CD architecture around some z_0 is given by,

$$\begin{aligned}\mathcal{H}_{\mu\phi} = \mathcal{B}_{\bar{k}_0} \int d\boldsymbol{\rho}\sigma\left(\boldsymbol{\rho},t\right) \\ \times\sum_{l,p}\int_0^\infty dk_0\left[A_{lp}^{(+)}\left(k_0\right)e^{ik_0(z_0-ct)}+h.c.\right] \\ \times\sum_{m,n}\int_0^\infty dk_0^{'}\left[A_{mn}^{(+)}\left(k_0^{\prime}\right)e^{ik_0^{\prime}(z_0-ct)}+h.c.\right],\end{aligned} \tag{A1}$$

where, $A_{lp}^{(+)}\left(k_0\right)=\hat{a}_{l,p}\left(k_0\right)\psi_{l,p}\left(\boldsymbol{\rho},z;k_0\right)$ and $\mathcal{B}_{\bar{k}_0}=C^2\left(\bar{k}_0\right)$ at the central frequency. When the Rayleigh range is long enough, we can take $k_0$to be constant throughout the integration over k_0 and absorb the factor due to $\int dk_0 e^{ik_0z_0}$ into the overall prefactor $\mathcal{A}$. For brevity we will omit the constants z_0 and k_0 from now on. We relabel the indices $(l,p)=\boldsymbol{k}$ and $(m,n)=\boldsymbol{n}$ and define the following projection integrals,

$$\theta_{\boldsymbol{nk}}\left(t\right)=\int d^2\boldsymbol{\rho}\psi_{\boldsymbol{n}}^*\left(\boldsymbol{\rho}\right)\sigma\left(\boldsymbol{\rho},t\right)\psi_{\boldsymbol{k}}\left(\boldsymbol{\rho}\right), \tag{A2}$$

$$\kappa_{\boldsymbol{nk}}\left(t\right)=\int d^2\boldsymbol{\rho}\psi_{\boldsymbol{n}}\left(\boldsymbol{\rho}\right)\sigma\left(\boldsymbol{\rho},t\right)\psi_{\boldsymbol{k}}\left(\boldsymbol{\rho}\right). \tag{A3}$$

When $\sigma\left(\boldsymbol{\rho},t\right)$ is time independent or varies slowly, $\kappa_{\boldsymbol{nk}}e^{\pm i2\omega_0t}$ terms that correspond to $a_{\boldsymbol{n}}a_{\boldsymbol{k}}$ and $a_{\boldsymbol{n}}^\dagger a_{\boldsymbol{k}}^\dagger$ are fast oscillating and self average while the cross terms show canceling phase contributions resulting in the Hamiltonian,

$$\mathcal{H}_{\mu\phi}=\mathcal{A}\sum_{\boldsymbol{n},\boldsymbol{k}}\theta_{\boldsymbol{nk}}a_{\boldsymbol{n}}^\dagger a_{\boldsymbol{k}}+\theta_{\boldsymbol{kn}}a_{\boldsymbol{n}}a_{\boldsymbol{k}}^\dagger, \tag{A4}$$

furthermore, the field Hamiltonian is further simplified as monochromatic and given in terms of the Schmidt bosons,

$$\begin{aligned}\mathcal{H}_\phi=\omega_0\sum_{\boldsymbol{n},\boldsymbol{k}}t_{\boldsymbol{nk}}a_{\boldsymbol{n}}^\dagger a_{\boldsymbol{k}}, \\ t_{\boldsymbol{nk}}=\int d^2\boldsymbol{\rho}\psi_{\boldsymbol{n}}^*\left(\boldsymbol{\rho}\right)\psi_{\boldsymbol{k}}\left(\boldsymbol{\rho}\right)=\delta_{\boldsymbol{nk}},\end{aligned}$$

which describes boson hopping on a lattice determined by the choice of basis. When the charge density is uniform $\theta_{\boldsymbol{nk}}$ only renormalize the Schmidt boson hopping term. This Hamiltonian is an interaction term between the HG or LG modes. The initial state of the light to be an entangled pair given by the Schmidt decomposition,

$$|\Psi\rangle=\sum_{\boldsymbol{n}}\sqrt{\lambda_{\boldsymbol{n}}}|\psi_{\boldsymbol{n}}\rangle_s|\psi_{\boldsymbol{n}}^*\rangle_i, \tag{A5}$$

where $\lambda_{\boldsymbol{n}}$ are the Schmidt coefficients and $|\psi_{\boldsymbol{n}}\rangle$ are the Schmidt modes. By modifying the degree of entanglement, we have control over the number of states that are effectively participating in the computation process. This can

be estimated by the Schmidt number $\kappa^{-1} = \sum_{\boldsymbol{n}} \lambda_{\boldsymbol{n}}^2$. One advantage of this setup is the ability to measure each state separately as well as functions of these states by projective measurement techniques available experimentally these days **? ?**]. Measuring each state separately corresponds to "local" observables while functions of them to "nonlocal" observables if we consider the Schmidt modes as bosons hoping on a lattice. Additional merit stems from unrestricted Hilbert space dimension that could be simulated. The Number of states is strictly controlled by the the degree of initial entanglement. The quantum calculation/simulator is not restricted to the number of entangled physical qubits, it is performed in the two-photon space which is in principle is infinite. Moreover, while reflection symmetry is persevered in the charge distribution, the system will model the dynamics of a closed quantum system (hermitian Hamiltonian). Anti-symmetric parts mimics open system dynamics (coupling to the environment). We stress that the coupling term between Schmidt bosons can be varied in time as well, this is an interesting feature for studying open and closed quantum systems out of equilibrium.

Appendix B: Effective Hamiltonian

We turn to the derivation of the effective Hamiltonian in which the photon-photon interaction term appears in a more intuitive manner. The Hamiltonian is given by,

$$\begin{aligned}\mathcal{H} &= H_0 + H_{\mu\phi} \\ &= \underbrace{H_\phi + H_\mu}_{H_0} + H_{\mu\phi},\end{aligned}$$

here $H_{\phi/\mu}$ represents the field/matter respectively and $H_{\mu\phi}$ is the interaction Hamiltonian. The interaction Hamiltonian can be written in the following form,

$$H_{\mu\phi} = \int d\boldsymbol{r}\hat{\sigma}\left(\boldsymbol{r}\right)\boldsymbol{A}^2\left(\boldsymbol{r}\right) \approx \sum_{\boldsymbol{kq}} \sigma^\dagger_{\boldsymbol{k-q}} a^\dagger_{\boldsymbol{k}} a_{\boldsymbol{q}} + \sigma_{\boldsymbol{k-q}} a_{\boldsymbol{k}} a^\dagger_{\boldsymbol{q}},$$

where the terms that are proportional to $a_{\boldsymbol{k}}a_{\boldsymbol{q}}, \left(a_{\boldsymbol{k}}a_{\boldsymbol{q}}\right)^\dagger$ where neglected. We model the charge density operator as,

$$\begin{aligned}\sigma\left(\boldsymbol{r}\right) &= \sum_{\alpha,i,j} w\left(\boldsymbol{r}-\boldsymbol{r}_\alpha\right) c^\dagger_{i,\alpha} c_{j,\alpha}, \\ \sigma_{\boldsymbol{k}} &= \sum_{\alpha=1}^{N} f_\alpha\left(\boldsymbol{k}\right) c^\dagger_{i,\alpha} c_{j,\alpha},\end{aligned}$$

such that $f_\alpha\left(\boldsymbol{k}\right) = e^{i\boldsymbol{k}\cdot\boldsymbol{r}_\alpha} w\left(\boldsymbol{k}\right)$ and w are the localized molecular orbital functions.

1. Schrieffer-Wolff transformation

In order to derive an effective interaction term between the photons we turn to the Schrieffer-Wolff transformation given by the rotation,

$$H' = e^S H e^{-S}.$$

Using the Baker-Campbell-Hausdorff formula we approximate the rotated Hamiltonian to,

$$H_{eff} = H + \left[S, H_0\right] + \frac{1}{2}\left[S, \left[S, H_0\right]\right] + ...$$

It is possible to use this expansion in order to derive the rotated Hamiltonian pertubatively. With the interesting choice $\left[S, H_0\right] = -H_{\mu\phi}$ we arrive to second order in the expansion the rotated Hamiltonian,

$$H_{eff} = H_0 + \frac{1}{2}\left[S, H_{\mu\phi}\right] + O\left(H_{\mu\phi}^3\right)$$

We start by computing the following commutation relations,

$$\begin{aligned}\eta &= \left[H_0, H_{\mu\phi}\right] \\ \eta_\phi + \eta_\mu &= \left[H_\phi, H_{\mu\phi}\right] + \left[H_\mu, H_{\mu\phi}\right],\end{aligned}$$

with the matter Hamiltonian $H_\mu = \sum_{\alpha,i} \epsilon_{i,\alpha} c_{i,\alpha}^\dagger c_{i,\alpha}$ counting bosonic excitations. For $\left[c_{i,\alpha}, c_{j,\beta}^\dagger\right] = \delta_{\alpha\beta}\delta_{i,j}$ and $(\hbar = 1)$ we obtain,

$$\begin{aligned}\eta_\phi &= \sum_{\boldsymbol{kq}} \left(\omega_{\boldsymbol{k}} - \omega_{\boldsymbol{q}}\right) \sigma_{\boldsymbol{k}-\boldsymbol{q}}^\dagger a_{\boldsymbol{k}}^\dagger a_{\boldsymbol{q}} + \left(\omega_{\boldsymbol{q}} - \omega_{\boldsymbol{k}}\right) \sigma_{\boldsymbol{k}-\boldsymbol{q}}^\dagger a_{\boldsymbol{k}} a_{\boldsymbol{q}}^\dagger, \\ \eta_\mu &= \sum_{\alpha,i,j,\boldsymbol{k},\boldsymbol{q}} \left(\epsilon_{i,\alpha} - \epsilon_{j,\alpha}\right) \left[f_\alpha^*\left(\boldsymbol{k}-\boldsymbol{q}\right) a_{\boldsymbol{k}}^\dagger a_{\boldsymbol{q}} + f_\alpha\left(\boldsymbol{k}-\boldsymbol{q}\right) a_{\boldsymbol{k}} a_{\boldsymbol{q}}^\dagger\right] c_{i,\alpha}^\dagger c_{j,\alpha},\end{aligned}$$

this allows us to derive the generator,

$$S = \sum_{\alpha,i,j,\boldsymbol{k},\boldsymbol{q}} \left[A_{\alpha ij}^{\boldsymbol{kq}} a_{\boldsymbol{k}}^\dagger a_{\boldsymbol{q}} + B_{\alpha ij}^{\boldsymbol{kq}} a_{\boldsymbol{k}} a_{\boldsymbol{q}}^\dagger\right] c_{i,\alpha}^\dagger c_{j,\alpha},$$

with the coupling tensors,

$$\begin{aligned}A_{\alpha ij}^{\boldsymbol{kq}} &= \frac{f_\alpha^*\left(\boldsymbol{k}-\boldsymbol{q}\right)}{\epsilon_{ij} + \Delta_{\boldsymbol{kq}}}, \\ B_{\alpha ij}^{\boldsymbol{kq}} &= \frac{f_\alpha\left(\boldsymbol{k}-\boldsymbol{q}\right)}{\epsilon_{ij} - \Delta_{\boldsymbol{kq}}},\end{aligned}$$

where $\Delta_{\boldsymbol{kq}} = \omega_{\boldsymbol{k}} - \omega_{\boldsymbol{q}}$ and $\epsilon_i - \epsilon_j = \epsilon_{ij}$. The effective Hamiltonian after tracing over the mater is given by,

$$\begin{aligned}H_{eff} &= H_\phi + \\ &+ 2 \sum_{\alpha\neq\beta} \sum_{\boldsymbol{k},\boldsymbol{q},\boldsymbol{s}} \frac{f_\alpha^*\left(\boldsymbol{k}-\boldsymbol{q}\right) f_\beta\left(\boldsymbol{s}-\boldsymbol{q}\right)}{\Delta_{\boldsymbol{kq}}} a_{\boldsymbol{k}}^\dagger a_{\boldsymbol{s}} + h.c. && \text{(B1a)} \\ &+ 2 \textstyle\sum_\alpha \displaystyle\sum_{\boldsymbol{k},\boldsymbol{q},\boldsymbol{s}} \left[f_\alpha\left(\boldsymbol{s}-\boldsymbol{q}\right) + f_\alpha^*\left(\boldsymbol{s}-\boldsymbol{q}\right)\right] \left[\frac{f_\alpha^*\left(\boldsymbol{k}-\boldsymbol{q}\right)}{\Delta_{\boldsymbol{kq}} + \epsilon_{ij}} a_{\boldsymbol{k}}^\dagger a_{\boldsymbol{s}} + \frac{f_\alpha\left(\boldsymbol{k}-\boldsymbol{q}\right)}{\Delta_{\boldsymbol{kq}} - \epsilon_{ij}} a_{\boldsymbol{s}}^\dagger a_{\boldsymbol{k}}\right] && \text{(B1b)} \\ &+ 8 \sum_{\alpha,i,j} \sum_{\boldsymbol{kqsr}} f_\alpha^*\left(\boldsymbol{k}-\boldsymbol{q}\right) f_\alpha^*\left(\boldsymbol{s}-\boldsymbol{r}\right) \frac{\epsilon_{ig}}{\Delta_{\boldsymbol{kq}}^2 - \epsilon_{ij}^2} a_{\boldsymbol{k}}^\dagger a_{\boldsymbol{q}} a_{\boldsymbol{r}}^\dagger a_{\boldsymbol{s}}. && \text{(B1c)}\end{aligned}$$

2. Derivation of the effective Schmidt-boson hamiltonian

The first term correspond to coherent, two-body mediated transport of momentum between radiation modes, the second term to incoherent, single-body transport of field momentum and the last correspond to photon-photon single-body-mediated interaction. We refer to hopping due to interaction with multiple (single) coherent (incoherent) hopping.

a. Coherent hopping

Assuming the paraxial limit, we approximate $\Delta_{\boldsymbol{kq}} \approx \frac{1}{2\omega_0}\left(k^2-q^2\right)$ where $k=|\boldsymbol{k}_\perp|, q=|\boldsymbol{q}_\perp|$, $c=\hbar=1$ and ω_0 is the central frequency in the longitudinal direction. To integrate the two-body mediated coherent hopping it is convenient to take the transverse angular variation of the orbital functions to be varying slowly. The exact term is given by,

$$t_{coh} = -\omega_0 \sum_{\alpha\neq\beta}\sum_{\boldsymbol{k},\boldsymbol{q}} e^{-i\boldsymbol{k}\cdot\boldsymbol{r}_\alpha + i\boldsymbol{q}\cdot\boldsymbol{r}_\beta} g_{kq}\left(\boldsymbol{r}_\alpha,\boldsymbol{r}_\beta\right) a^\dagger_{\boldsymbol{k}} a_{\boldsymbol{q}} + h.c., \tag{B2}$$

where,

$$g_{kq}\left(\boldsymbol{r}_\alpha,\boldsymbol{r}_\beta\right) = 2\int d^2\boldsymbol{q}' \frac{w^*_\alpha\left(\boldsymbol{k}-\boldsymbol{q}'\right) w_\beta\left(\boldsymbol{q}-\boldsymbol{q}'\right)}{q'^2-k^2} e^{-i\boldsymbol{q}'\cdot\left(\boldsymbol{r}_\beta-\boldsymbol{r}_\alpha\right)}, \tag{B3}$$

In the point particle approximation we obtain,

$$g_{kq}\left(\boldsymbol{r}_\alpha,\boldsymbol{r}_\beta\right) \approx 2\int q' dq' \frac{J_0\left(q' r_{\beta\alpha}\right)}{q'^2-k^2}. \tag{B4}$$

In the next section we will integrate over the continuous wavevector and end up with discrete Schmidt boson operators. g^{coh}_{kq} is carefully regularized with the cutoff Λ, $g^{coh}_{kq} = 2\int_{1/\Lambda}^{\Lambda} dq \frac{\sin(q)}{q'^2-(r_{\beta\alpha}k)^2}$. When $r_{\beta\alpha}/\Lambda \leq r_{\beta\alpha}k \ll 1$ and $q > 1/\Lambda$ it is instructive to imagine a setup in which $|r_{\alpha\beta}| \ll \lambda_\perp$ such that the $J_0 \approx 1$ is flat and the renormalized coherent hopping carry the spatial contribution due to the phase-difference resulting in,

$$g_{kq}\left(\boldsymbol{r}_\alpha,\boldsymbol{r}_\beta\right) \approx g^{coh}, \tag{B5}$$

and the point charge approximation results in,

$$t_{coh} = -\omega_0 g^{coh} \sum_{\boldsymbol{k},\boldsymbol{q}} S_{\boldsymbol{kq}} a^\dagger_{\boldsymbol{k}} a_{\boldsymbol{q}} + h.c., \tag{B6}$$

where $S_{\boldsymbol{kq}} = \sum_{\alpha\neq\beta} e^{-i\boldsymbol{k}\cdot\boldsymbol{r}_\alpha + i\boldsymbol{q}\cdot\boldsymbol{r}_\beta}$ is the geometric structure factor that vanishes for disordered geometries and dominates when there is long range order.

b. Incoherent hopping

Similarly, neglecting the highly oscillatory terms and carry with the integration of the hopping term (II) we obtain,

$$t_{inc} = -\omega_0 \sum_{\alpha,i,\boldsymbol{k},\boldsymbol{q}} \left[g^{inc}_{kq}\left(\Delta_i\right) e^{-i(\boldsymbol{k}-\boldsymbol{q})\cdot\boldsymbol{r}_\alpha} a^\dagger_{\boldsymbol{k}} a_{\boldsymbol{q}} + g^{inc*}_{kq}\left(-\Delta_i\right) e^{i(\boldsymbol{k}-\boldsymbol{q})\cdot\boldsymbol{r}_\alpha} a^\dagger_{\boldsymbol{q}} a_{\boldsymbol{k}} \right], \tag{B7}$$

where $\Delta_i = 2\omega_0\epsilon_{ig}$ and the integration over the localized molecular orbitals is given by,

$$g^{inc}_{ks}\left(\Delta_i\right) = 2\int d^2\boldsymbol{q} \frac{w^*_\alpha\left(\boldsymbol{k}-\boldsymbol{q}\right) w_\alpha\left(\boldsymbol{s}-\boldsymbol{q}\right)}{q^2-\left(k^2+\Delta_i\right)}, \tag{B8}$$

and the radial component can be carried via analytical continuation to the complex plane. When the momentum distribution of the molecular orbital functions is uniform in the integration region (point particle limit), $\sum_i g^{inc}_{ks}\left(\Delta_i\right) = g_{inc}$ in a similar procedure to the coherent hopping. The incoherent hopping term is finally given by,

$$t_{inc} = -\omega_0 g_{inc} \sum_{\alpha,\boldsymbol{k},\boldsymbol{q}} e^{-i(\boldsymbol{k}-\boldsymbol{q})\cdot\boldsymbol{r}_\alpha} a^\dagger_{\boldsymbol{k}} a_{\boldsymbol{q}} + h.c. \tag{B9}$$

3. Schmidt-Boson representation

Using the above definitions for the Bogoliubov transformation from momentum space to the Schmidt representation,

$$a_{\boldsymbol{k}} = \sum_n \phi_n(\boldsymbol{k})\, a_n, \tag{B10}$$

where a_n is the Schmidt boson annihilation operator. The free Hamiltonian reads,

$$H_\phi = \sum_{\boldsymbol{k}} \omega_{\boldsymbol{k}} a^\dagger_{\boldsymbol{k}} a_{\boldsymbol{k}}, \tag{B11}$$

assuming a single longitudinal mode ω_0 we get,

$$H_\phi = \omega_0 \sum_n a^\dagger_n a_n. \tag{B12}$$

a. Hopping

The modal-hopping reads,

$$t_{coh} = -\omega_0 \sum_{nm} \theta^{coh}_{nm} a^\dagger_n a_m + h.c., \tag{B13}$$

$$\theta^{coh}_{nm} = \sum_{\alpha\neq\beta} e^{-i\boldsymbol{k}\cdot\boldsymbol{r}_\alpha + i\boldsymbol{q}\cdot\boldsymbol{r}_\beta} g_{kq}(\boldsymbol{r}_\alpha, \boldsymbol{r}_\beta)\, \phi^*_n(\boldsymbol{k})\, \phi_m(\boldsymbol{q}), \tag{B14}$$

where ψ_n is the real-space representation of ϕ_n. This simplifies further in the point-particle limit,

$$\theta^{coh}_{nm} = g^{coh} \sum_{\alpha\neq\beta} \psi^*_n(\boldsymbol{r}_\alpha)\, \psi_m(\boldsymbol{r}_\beta). \tag{B15}$$

The incoherent hopping similarly reads,

$$t_{inc} = -\omega_0 \sum_{n,k} \theta^{inc}_{nk} a^\dagger_n a_k + h.c., \tag{B16}$$

$$\theta^{inc}_{nk} = g^{inc} \sum_{\alpha} \psi^*_n(r_\alpha)\, \psi_m(r_\alpha), \tag{B17}$$

The over-all Schmidt-boson transport coefficient is given by,

$$t_{nk} = \omega_0 \left(\delta_{nk} - \theta^{coh}_{nk} - \theta^{inc}_{nk}\right),$$

and the Hamiltonian is,

$$H_{eff} = \sum_{n,k} t_{nk} a^\dagger_n a_k + h.c. + H_{\phi-\phi}.$$

b. Interaction

We define the terms,

$$V_{nm}^{1,\alpha}\left(\epsilon_{ig}\right)=\int d^{2}\boldsymbol{k}d^{2}\boldsymbol{q}e^{-i(\boldsymbol{k}-\boldsymbol{q})\cdot\boldsymbol{r}_{\alpha}}\frac{\phi_{n}^{*}\left(\boldsymbol{k}\right)\phi_{m}\left(\boldsymbol{q}\right)}{q^{2}-k^{2}+\Delta_{i}}, \tag{B18}$$

$$f_{nm}^{\alpha}=\psi_{n}^{*}\left(r_{\alpha}\right)\psi_{m}\left(r_{\alpha}\right), \tag{B19}$$

and rewrite the interaction term as,

$$\begin{aligned}U_{nmls}=-4\sum_{\alpha}\int d^{2}\boldsymbol{k}d^{2}\boldsymbol{q}d^{2}\boldsymbol{k}'d^{2}\boldsymbol{q}'e^{-i(\boldsymbol{k}-\boldsymbol{q})\cdot\boldsymbol{r}_{\alpha}}e^{-i\left(\boldsymbol{k}'-\boldsymbol{q}'\right)\cdot\boldsymbol{r}_{\alpha}}\\ \times\left[\frac{1}{k^{2}-q^{2}-\Delta_{i}}-\frac{1}{k^{2}-q^{2}+\Delta_{i}}\right]\phi_{n}^{*}\left(\boldsymbol{k}\right)\phi_{m}\left(\boldsymbol{q}\right)\phi_{l}^{*}\left(\boldsymbol{k}'\right)\phi_{s}\left(\boldsymbol{q}'\right)\end{aligned} \tag{B20}$$

and recall the identity,

$$e^{i\boldsymbol{k}\cdot\boldsymbol{r}_{\alpha}}=\sum_{n}\phi_{n}^{*}\left(\boldsymbol{k}\right)\psi_{n}\left(\boldsymbol{r}_{\alpha}\right), \tag{B21}$$

then sum the prime coordinates and rewrite the exponents as sums of the spatial modes,

$$-4\int d^{2}\boldsymbol{k}d^{2}\boldsymbol{q}\left[\frac{1}{k^{2}-q^{2}-\epsilon_{ig}}-\frac{1}{k^{2}-q^{2}+\epsilon_{ig}}\right]\phi_{n}^{*}\left(\boldsymbol{k}\right)\phi_{m}\left(\boldsymbol{q}\right)\sum_{\alpha}e^{-i(\boldsymbol{k}-\boldsymbol{q})\cdot\boldsymbol{r}_{\alpha}}\psi_{l}^{*}\left(\boldsymbol{r}_{\alpha}\right)\psi_{s}\left(\boldsymbol{r}_{\alpha}\right)$$

rewriting the exponent using Eq.B21 the interaction is given by,

$$\begin{aligned}\sum_{\alpha}e^{-i(\boldsymbol{k}-\boldsymbol{q})\cdot\boldsymbol{r}_{\alpha}}\psi_{l}^{*}\left(\boldsymbol{r}_{\alpha}\right)\psi_{s}\left(\boldsymbol{r}_{\alpha}\right)&=\sum_{\alpha}\left[\sum_{l'}\phi_{l'}^{*}\left(\boldsymbol{k}\right)\psi_{l}'\left(\boldsymbol{r}_{\alpha}\right)\psi_{l}\left(\boldsymbol{r}_{\alpha}\right)\right]^{*}\left[\sum_{s'}\phi_{s'}^{*}\left(\boldsymbol{q}\right)\psi_{s'}\left(\boldsymbol{r}_{\alpha}\right)\psi_{s}\left(\boldsymbol{r}_{\alpha}\right)\right]\\&=\sum_{l's'}\phi_{l'}\left(\boldsymbol{k}\right)\phi_{s'}^{*}\left(\boldsymbol{q}\right)\sum_{\alpha}f_{ll'}^{\alpha*}f_{ss'}^{\alpha},\end{aligned} \tag{B22}$$

recasting the interaction term,

$$\begin{aligned}U_{nmls}=-4\sum_{l's'}\sum_{\alpha,i}f_{ll'}^{\alpha*}f_{ss'}^{\alpha}\int d^{2}\boldsymbol{k}d^{2}\boldsymbol{q}\\ \times\phi_{n}^{*}\left(\boldsymbol{k}\right)\phi_{l'}\left(\boldsymbol{k}\right)\left[\frac{1}{k^{2}-q^{2}-\Delta_{i}}-\frac{1}{k^{2}-q^{2}+\Delta_{i}}\right]\phi_{m}\left(\boldsymbol{q}\right)\phi_{s'}^{*}\left(\boldsymbol{q}\right),\end{aligned} \tag{B23}$$

This is the exact (basis dependent) effective interaction term. The four modes scattering on this potential is a property of the chosen basis. The structure factors f_{nm}^{α} hold the geometric dependency of the effective interaction which can be designed. It is convenient to define the scattering potential,

$$\begin{aligned}V_{nlkm}=\int d^{2}\boldsymbol{k}d^{2}\boldsymbol{q}\\ \times\phi_{n}^{*}\left(\boldsymbol{k}\right)\phi_{k}\left(\boldsymbol{k}\right)\left[\frac{1}{k^{2}-q^{2}-\Delta_{i}}-\frac{1}{k^{2}-q^{2}+\Delta_{i}}\right]\phi_{l}\left(\boldsymbol{q}\right)\phi_{m}^{*}\left(\boldsymbol{q}\right),\end{aligned} \tag{B24}$$

and the geometric structure factor,

$$S_{ll'ss'}=\sum_{\alpha,i}f_{ll'}^{\alpha*}f_{ss'}^{\alpha} \tag{B25}$$

isolating basis dependent properties from the geometrical characteristics,

$$U_{nmls} = -\sum_{l's'} S_{ll'ss'} V_{nml's'}, \tag{B26}$$

allowing one to study them separately. The effective Hamiltonian is finally given by,

$$H_{eff} = \sum_{n,k} t_{nk} a_n^\dagger a_k - \sum_{nklm} U_{nklm} a_n^\dagger a_k a_l^\dagger a_m. \tag{B27}$$

4. LG basis

We now recall that each SB has two quantum numbers. For LG modes we can carry the integration over the azimuthal dimension such that $n \to n_r, n_o$ for the radial and azimuthal DOF,

$$\begin{aligned} &-4\sum_{l's'} \int kdkqdq \left[\frac{1}{k^2-q^2-\Delta} - \frac{1}{k^2-q^2+\Delta}\right] \phi^*_{n_r}(k)\,\phi_{l'_r}(k)\,\phi_{m_r}(q)\,\phi^*_{s'_r}(q) \\ &\times\delta_{n_o,l'_o}\delta_{m_o,s'_o} \sum_\alpha f^{\alpha *}_{ll'} f^\alpha_{ss'} \left[e^{-i\pi\left(n_r-l'_r\right)} e^{i\pi\left(m_r-s'_r\right)}\right] \end{aligned}$$

by exchanging $k \leftrightarrow q$ for the second term in the brackets (negative contribution) absorbing the minus sign we get,

$$\begin{aligned} &-4\sum_{l's'} \int kdkqdq \left[\frac{1}{k^2-q^2-\Delta}\right] \left[\phi^*_{n_r}(k)\,\phi_{l'_r}(k)\,\phi_{m_r}(q)\,\phi^*_{s'_r}(q) + \phi^*_{n_r}(q)\,\phi_{l'_r}(q)\,\phi_{m_r}(k)\,\phi^*_{s'_r}(k)\right] \\ &\times\delta_{n_o,l'_o}\delta_{m_o,s'_o} \sum_\alpha f^{\alpha *}_{ll'} f^\alpha_{ss'} \left[e^{-i\pi\left(n_r-l'_r\right)} e^{i\pi\left(m_r-s'_r\right)}\right]. \end{aligned}$$

We can simplify this expression further using an analytical continuation of k and write,

$$\frac{1}{k^2-q^2-\Delta} = \lim_{\delta\to 0} \frac{1/k+\sqrt{q^2+\Delta}}{k-\sqrt{q^2+\Delta}-i\delta},$$

and perform the integration over k resulting in using the Sokhotski–Plemelj theorem,

$$\begin{aligned} U_{nmls} =& -2\pi\sum_{l's'} \int qdq \\ &\left[\phi^*_{n_r}\left(\sqrt{q^2+\Delta}\right)\phi_{l'_r}\left(\sqrt{q^2+\Delta}\right)\phi_{m_r}(q)\,\phi^*_{s'_r}(q) + \phi^*_{n_r}(q)\,\phi_{l'_r}(q)\,\phi_{m_r}\left(\sqrt{q^2+\Delta}\right)\phi^*_{s'_r}\left(\sqrt{q^2+\Delta}\right)\right] \\ &\times\delta_{n_o,l'_o}\delta_{m_o,s'_o} \sum_\alpha f^{\alpha *}_{ll'} f^\alpha_{ss'} \left[e^{-i\pi\left(n_r-l'_r\right)} e^{i\pi\left(m_r-s'_r\right)}\right]. \end{aligned} \tag{B28}$$

When Δ is large this vanishes, only $q^2 > \Delta$ contribute to the effective interaction. From the general form of the Fourier transform of the LG modes at $z = 0$ we can see exponential suppression of these modes when they are translated,

$$\phi_{lp}(q,\varphi) = \sqrt{\frac{p!}{2\pi\,(|l|+p)!}} \left(\frac{q}{\sqrt{2}}\right)^{|l|} L_P^{|l|}\left(\frac{q^2}{2}\right) e^{-\frac{q^2}{4}} e^{il\varphi} e^{-i\frac{\pi}{2}(2p+|l|)},$$

where the last phase factor is responsible for the sign changing term that appeared after the azimuthal integration, and we have beam waist $w_0 = 1$.